HyperU-Mesh: Real-time deformation of soft-tissues across variable patient-specific parameters

Sidaty El Hadramy, Nicolas Padoy, Stéphane Cotin

HyperU-Mesh: Real-time deformation of soft-tissues across variable patient-specific parameters

Sidaty El hadramy[1,2], Nicolas Padoy[2,3], and Stéphane Cotin[1,2]

[1] Inria, Strasbourg, France.
[2] ICube, University of Strasbourg, Strasbourg, CNRS, France.
[3] IHU Strasbourg, Strasbourg, France.

Abstract. Physics-based Patient-Specific Biomechanical models (PSBMs), particularly those using finite element methods (FEM), simulate organ behaviors accurately but are computationally intensive, especially for hyper-elastic tissues. To address this, U-Mesh [13] introduced a data-driven approach using U-Net architecture, achieving real-time inference but reliant on precise stiffness knowledge at training. This paper introduces HyperU-Mesh, an extension that integrates a Hypernetwork to condition U-Mesh based on stiffness prior distributions. By training with FEM-simulated data that varies stiffness under a predefined distribution, HyperU-Mesh ensures accuracy across variable stiffness without retraining. Experimental results highlight its effectiveness across different scenarios, showing comparable accuracy to FEM while significantly improving speed.

Keywords: Physics-based biomechanical models, Deep Learning, HyperNetworks

1 Introduction

In healthcare, digital twins (DTs) are virtual replicas of human organs and/or systems created using diverse medical imaging data [1]. Their application goes from training clinicians to intraoperative guidance. Several studies have demonstrated the benefits of physics-based digital twins [2–4], in particular, Patient-Specific Biomechanical models (PSBMs) for their accuracy and predictive ability over sparse and/or noisy intraoperative data. PSBMs are usually based on the principles of continuum mechanics, often employing finite element methods (FEM) to solve the numerical system describing the physical behavior of the organ or system. While these models provide precise simulations of organ and system behaviors, their computational complexity often results in time-consuming calculations, especially when involving soft tissue hyper-elastic behavior [5]. This limits their use in computer-assisted interventions, delaying real-time guidance during surgical procedures and complicating their effective integration. Therefore, significant efforts are being directed toward optimizing these models to enhance both the accuracy and computational speed of PSBMs, addressing these critical limitations [5].

Various trade-offs between the speed and accuracy of PSBMs have been proposed [3, 6, 7, 13]. Haouchine et al. [3] suggested using a co-rotational model to handle large deformations with small strain. Yet, their approach significantly loses accuracy when advanced biomechanical laws are considered. Depending on the acceptable level of accuracy loss, reducing the model's degrees of freedom is a viable strategy to meet real-time

constraints. Methods such as Proper Orthogonal Decomposition (POD) [6] and Proper Generalized Decomposition (PGD) [7] have been proposed for this purpose. Another category of methods leverages the high number of cores available in Graphics Processing Units (GPUs) for parallel computing, which enables significant speedups in handling computationally intensive problems [8]. Deep neural network architectures have recently demonstrated strong capabilities in learning complex, high-level nonlinear relationships between diverse input-output data [9, 10]. One of the strengths of these networks is their ability to accurately perform inference in real-time when trained with sufficient data. Several works have proposed to train deep neural networks on simulated (using FEM) data [11–14], aiming to learn the behavior of PSBMs. Among them, U-Mesh, introduced by Mendizabal et al. [13], stands out as a simple yet effective solution.

U-Mesh is a data-driven approach based on a U-Net [15] architecture, designed to approximate the nonlinear relationship between forces and displacement fields. It is trained in a patient-specific manner using simulated data generated by Finite Element Method (FEM) and achieves real-time performance during inference. U-Mesh [13] has shown strong performance on real-world data, making it a promising approach in terms of both accuracy and speed. However, U-Mesh is trained on a single value of material stiffness. Hence, its accuracy at inference time depends on precise knowledge of patient-specific stiffness during training. This dependency limits its application in computer-assisted interventions, as such material parameters of organs are often available only during the intervention using techniques such as FibroScan®. This paper introduces HyperU-Mesh, an extended version of U-Mesh that incorporates conditioning on a distribution of material stiffness. This approach ensures that HyperU-Mesh maintains accuracy even when the stiffness is only known at inference time. Conditioning is achieved using a Hypernetwork [16], which generates a unique set of weights for U-Mesh based on the given stiffness value at inference time. HyperU-Mesh is trained on data simulated using the Finite Element Method (FEM). However, we generate samples where the material stiffness varies according to a specified prior distribution. The structure of the paper is as follows: Section 2 outlines our methodology. Section 3 illustrates its effectiveness in two distinct scenarios with varying tissue properties and domain geometries. Section 4 discusses our findings. Finally, Section 5 concludes the paper and explores future research directions.

2 HyperU-Mesh

Hypernetworks [16] are an approach where one network, referred to as the hypernetwork, generates the weights for another network, known as the primary network. This allows the primary network's weights to be dynamically adjusted during inference based on specific conditions inputted to the hypernetwork. Therefore, they have emerged as a way to enhance the flexibility and performance of deep neural networks [17]. We introduce HyperU-Mesh, an improved version of U-Mesh [13], incorporating a hypernetwork to integrate patient-specific stiffness information. An overview of HyperU-Mesh is illustrated in the figure 1. We use U-Mesh as a primary network that takes as input the forces, denoted F, and predicts the relative displacement field u. A 4-layer Multi-Layer Perceptron h predicts weights $d\theta$ for a given stiffness value λ.

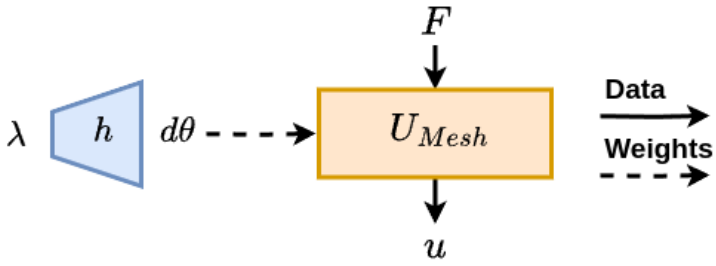

Fig. 1: Overview of HyperU-Mesh: U-Mesh [13] serves as the primary network, taking forces F as input to predict u, the relative displacement field. A hypernetwork h enhances U-Mesh's predictions by incorporating stiffness information. Both networks are trained end-to-end using data generated with FEM simulations.

Training hypernetworks is often challenging, particularly due to the proportionality between input and output magnitudes, which leads to very slow convergence. Ortiz et al. [18] identified and resolved this issue by treating the predicted weights as additive changes for the primary network. For a given training iteration n, the weights $d\theta_n$ predicted by the hypernetwork h are used to update the weights of the primary network (U-Mesh) following the equation below:

$$\theta_n = \theta_0 + d\theta_n \tag{1}$$

With θ_0 the initial weights of the U-Mesh. Unlike traditional hypernetworks [16], the weights θ_0 are also trainable parameters. The weights $d\theta_n$ influence the predictions of the U-Mesh by incorporating knowledge of the stiffness λ. This strategy permits a better initialization of the primary network weights, which leads to fast and efficient training of the U-Mesh. Typically, the training time of the approach is comparable to the training time of the primary network without a hypernetwork. h takes as input a parameter set λ that describes stiffness, varying depending on the specific biomechanical law used. For example, in the context of the Saint-Venant Kirchhoff constitutive law, λ corresponds to Young's modulus. The output of h has the same size as the number of parameters in the U-Mesh. We conducted an ablation study on the original version proposed by Mendizabal et al. [13] to decrease its weight count. As a result, without any loss of accuracy, we reduced the number of weights in the initial U-Mesh architecture by 4 by removing its unnecessary layers.

HyperU-Mesh is trained in an end-to-end manner using training data generated via FEM. Unlike U-Mesh, we generate training data by varying the stiffness parameter(s) according to a selected prior distribution from the literature. The training process optimizes the weights of both networks by minimizing the Mean Square Error (MSE) between the prediction and ground truth displacement fields.

3 Experiments

To evaluate our method, we conducted two experiments on two different geometries with distinct material properties. HyperU-Mesh is implemented with PyTorch[4]. We utilized Adam Optimizer with a learning rate of 10^{-5}. The FEM simulations were performed using the SOFA Framework [19] with the SOniCS [20] plugin for soft-tissue biomechanics. Computation was carried out using an Nvidia Titan RTX GPU. As a metric, we use classical Hausdorff distance in millimeters and the relative Hausdorff distance, defined as the percentage error relative to the deformation amplitude. Both metrics are computed using the implementation from SciPy[5]. We also report the computation time for a prediction.

3.1 PDMS Beam

We aim to estimate the deformation of a PolyDiMethylSiloxane (PDMS) beam under gravity, with the left end fixed to a vertical support, as illustrated in the left image of Figure 2. This example, adapted from Mazier et al. [21], involves characterizing the material behavior using the Mach-1™ mechanical testing system (Biomomentum, Canada) for unconfined compression tests. The material is best approximated by a Mooney-Rivlin model with $C_{01} = 101$ kPa and $C_{10} = 151$ kPa. For validation, we obtained the ground truth deformation data from Mazier et al. [21].

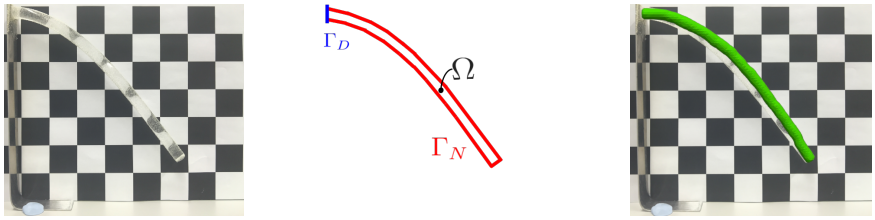

Fig. 2: **Left**: the observed deformation of the beam, fixed on the left side and deforming under gravity. **Middle**: An illustration of the simulation domain **Right**: The prediction of HyperU-Mesh (in green) overlaid onto the ground truth beam.

Finite element simulation: We formulate a boundary value problem for computing the deformation of a hyperelastic material under both Dirichlet and Neumann boundary conditions (BCs). The beam occupies a volume Ω with boundary Γ. The Dirichlet and Neumann boundary conditions are on Γ_D and Γ_N, two subsets of Γ. These domains are illustrated in the middle image of Figure 2. The elastic properties of soft tissues can be characterized using principles from continuum mechanics. By employing the

[4] https://pytorch.org/docs/stable/index.html
[5] https://docs.scipy.org/doc/scipy/index.html

Lagrangian formulation, the relationship between the deformed (x) and undeformed (X) states, at each point along the beam can be expressed as

$$\mathrm{x} = \mathrm{X} + \mathrm{u} \tag{2}$$

Where u is the displacement field. The deformation gradient tensor $\boldsymbol{F} = \mathrm{I} + \nabla_{\mathrm{X}} u$, provides a local description of the deformation and the Green-Lagrange strain tensor $\boldsymbol{E} \in \mathrm{R}^{3\times3}$ as expressed following equation 3

$$\boldsymbol{E} = \frac{1}{2}(\boldsymbol{C} - \boldsymbol{I}) \tag{3}$$

Where $\boldsymbol{C} = F^T F$ is called the right Cauchy-Green deformation tensor and $\boldsymbol{I}$ the identity matrix. The material behaviour is approximated with a nearly incompressible Mooney-Rivlin [21] with parameters C_{01}, C_{10} and D_1, the strain-energy density function W is expressed as:

$$\mathrm{W} = C_{01}(J^{-\frac{2}{3}}\mathrm{I}_{\mathbf{C}} - 3) + C_{10}(J^{-\frac{4}{3}}\mathrm{II}_{\mathbf{C}} - 3) + \frac{\ln(\mathrm{J})}{2D_1} \tag{4}$$

In equation 4, J is the jacobian matrix, while $\mathrm{I}_{\mathbf{C}} = \mathrm{tr}(\boldsymbol{C})$ and $\mathrm{II}_{\mathbf{C}} = \frac{1}{2}\left((\mathrm{tr}(\mathbf{C}))^2 - \mathrm{tr}\left(\mathbf{C}^2\right)\right)$ are the classic invariants. The stress-strain relationship, also known as constitutive law, is obtained by differentiating $\mathbf{W}$ with respect to $\mathbf{C}$, see equation 5

$$\mathbf{S} = 2\frac{\partial \mathbf{W}}{\partial \mathbf{C}} \tag{5}$$

With S being the second Piola-Kirchhoff stress tensor. The boundary value problem is then formulated as in equation 3, where g represents the body forces, n the unit normal to Γ_N, and t the traction forces applied on Γ_N domain.

$$\begin{cases} \nabla(FS) = g \quad \text{on} \quad \Omega \\ u(X) = 0 \quad \text{on} \quad \Gamma_D \\ (FS)n = t \quad \text{on} \quad \Gamma_N \end{cases} \tag{6}$$

The domain Ω is discretized wth hexahedral elements. This is motivated by their good convergence property, lock-free behavior and regular structure that fits well Convolutional Neural Networks (CNN) inputs [22]. The equation 6 is solved with the FEM to find the relative displacement field.

Training data generation: We generated 1,000 training samples using the finite element simulation described earlier. For each sample, body forces were selected from a uniform distribution over [−15 N, −7 N], while the material parameters C_{01} and C_{10} were both sampled from uniform distributions over [100 kPa, 200 kPa]. The Dirichlet domain Γ_D remained fixed across all simulations. The relative displacement field for each dataset sample was obtained through the finite element simulation outlined earlier. A sample from the dataset includes the body forces F as input for U-Mesh, the relative displacement field u to supervise U-Mesh's prediction, and the material properties $\lambda = [C_{01}, C_{10}]$, which serve as the input for the hypernetwork h.

Results: HyperU-Mesh was trained during 100 epochs on the 6, 000 generated samples, with a batch size of 1. We used an MSE between the prediction and the ground truth displacement fields as a loss function. Upon training, we tested HyperU-Mesh in the case where the body forces are equal to -9.81 N and the material parameters are: $C_{01} = 101$ kPa, $C_{10} = 151$ kPa and $D_1 = 7.965 \times 10^{-5}$ kPa. The predicted deformation (illustrated in the rightmost image of Figure 2) is compared with the ground truth real deformation provided by Mazier et al. [21]. Table 1 presents the numerical results, including the performance of U-Mesh [13], where all training was conducted with known material parameters. The table also compares the results of a FEM simulation to the ground truth deformation. The experiment demonstrates that HyperU-Mesh achieves comparable accuracy to both standard FEM and U-Mesh while operating 750 times faster than standard FEM. HyperU-Mesh also showcases versatility across a distribution of material parameters, unlike U-Mesh, which is constrained to a single known value required during training.

	Hausdorff (mm)	**Relative Hausdorff (%)**	**Time (ms)**
FEM	**4.7**	**3.6**	**3000**
U-Mesh [13]	**5.3**	**4.1**	**4**
HyperU-Mesh	**5.6**	**4.3**	**4**

Table 1: Results from the beam experiments, shows comparisons between predictions made by standard FEM, U-Mesh, and HyperU-Mesh against the ground truth deformation. HyperU-Mesh achieves results comparable to both state-of-the-art methods while operating 750 times faster than standard FEM and offering greater flexibility than U-Mesh [13] in handling diverse material properties.

3.2 Human liver

In this experiment, we aim to estimate the deformation of an ex-vivo human liver subjected to a force estimated to 5.1 N applied to the right lobe, the rest and deformed states of the liver are illustrated in Figure 3. The geometries of both liver states are retrieved from a segmented CT scan. The stiffness of the organ was measured with a FibroScan® and estimated to be 7 kPa.

Finite element simulation: Similar to the beam experiment, we formulate a boundary value problem to compute the deformation of soft tissue under both Dirichlet and Neumann boundary conditions. The underlying physics remains consistent with the beam case, except for the material behavior, which is approximated here using a Saint-Venant-Kirchhoff model. Thus, the strain energy density function is expressed as follows:

$$\mathrm{W} = \frac{\lambda}{2}[tr(E)]^2 + \mu tr(E^2) \tag{7}$$

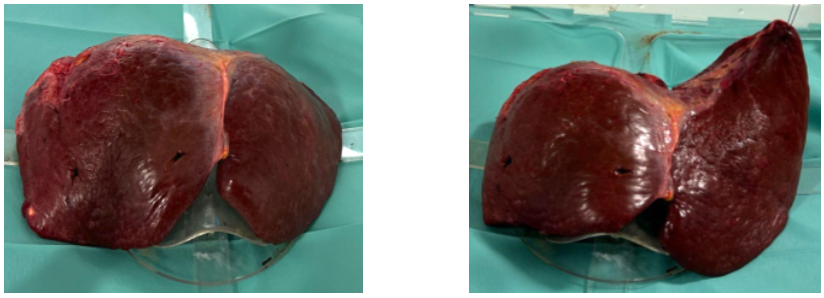

Fig. 3: Rest and deformed states of the ex-vivo liver.

In equation 7, E is the Green-Lagrange strain tensor, λ, and μ are Lamé's first and second parameters that are related to the Young modulus and Poisson ration. In Figure 3, the Dirichlet domain is selected at the junction between the parenchyma and the portal vein. Traction forces are applied on the Neumann domain, which is chosen on the organ's surface.

Training data generation: Using finite element simulation, we generated 3,000 synthetic deformations of the organ. For each deformation, we randomly selected a location on the liver surface to apply traction forces, which were sampled from a uniform distribution over [2 N, 10 N]. Additionally, Young's modulus was sampled from a uniform distribution over [5000 Pa, 12000 Pa] for each generated sample. Consequently, a sample from the dataset includes the applied forces Fas input for U-Mesh, the chosen Young's modulus as the input λ of the hypernetwork h, and the relative displacement field obtained through FEM, which serves as the ground truth to supervise U-Mesh's prediction u.

Results: HyperU-Mesh was trained for 100 epochs on 3000 synthetic deformations of the liver with a batch size of 1. We used an MSE loss function between the predicted and FEM displacement fields to supervise the training. After training, we tested HyperU-Mesh with applied forces of 5.1N at the right lobe and a Young Modulus of 7 kPa. The predicted deformation was compared to the ground truth deformation, and the results are presented in Table 2. The leftmost image in Figure 4 shows the geometry predicted by HyperU-Mesh superimposed on an image of the ground truth deformation. As one may notice, the errors in this experiment for HyperU-Mesh and other methods are higher than in the previous one. We attribute this to the uncertainty related to estimating the fixed boundary conditions. However, HyperU-Mesh achieves comparable results with U-Mesh and FEM, while being faster than FEM and more flexible (on material properties) than U-Mesh. To further evaluate the robustness of our method, we compared HyperU-Mesh predictions with standard FEM solutions over 100 synthetic deformations, resulting in a Mean Absolute Error (MAE) of 1.77 mm $\pm$ 0.82 mm. The rightmost image of Figure 4 highlights a comparison between HyperU-Mesh and FEM predictions on a synthetic deformation.

	Hausdorff (mm)	Relative Hausdorff (%)	Time (ms)
FEM	**15.1**	**11.6**	**500**
U-Mesh [13]	**16.6**	**12.7**	**4**
HyperU-Mesh	**16.5**	**12.6**	**4**

Table 2: Results of the liver experiments compare the predictions of standard FEM, U-Mesh, and HyperU-Mesh against the ground truth deformation. HyperU-Mesh achieves results comparable to both state-of-the-art methods while being significantly times faster than standard FEM and more versatile than U-Mesh [13] in handling a range of material properties.

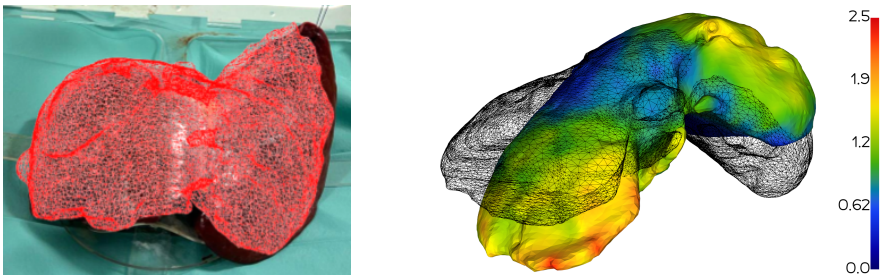

Fig. 4: **Left**: Prediction of HyperU-Mesh (in red) superimposed on the ground truth deformation. **Right**: The wireframe illustrates the rest shape of the liver. The heatmap displays the prediction of HyperU-Mesh on a synthetic deformation, highlighting the error in millimeters compared to the FEM solution.

4 Discussion

Results show that HyperU-Mesh is a promising approach, particularly in scenarios involving complex material properties and anatomical structures. The experiments demonstrated that HyperU-Mesh achieves comparable accuracy to both standard FEM and U-Mesh while operating significantly faster than standard FEM. Moreover, unlike U-Mesh, which is limited to a single value of material parameters known at training time, HyperU-Mesh demonstrates versatility over a distribution of material parameters. This flexibility allows HyperU-Mesh to adapt to patient-specific material properties intraoperatively, enhancing its robustness and reliability in clinical applications where such variations are prevalent. However, the liver, being a complex organ with varying mechanical properties and physiological states, presents difficulties in accurately defining boundary conditions. The uncertainties associated with fixed boundary conditions can lead to increased errors across all modeling methods, as observed in experiment 2. Therefore, while HyperU-Mesh shows promise in enhancing the efficiency and accuracy of biomechanical simulations, particularly in liver modeling, several challenges remain, including handling uncertain boundary conditions. Addressing these challenges will be crucial in realizing the full potential of HyperU-Mesh in clinical practice.

5 Conclusion

In this paper, we introduced HyperU-Mesh, an extension of the U-Mesh [13] framework designed to enhance the accuracy, speed, and flexibility of physics-based biomechanical models (PSBMs) in real-time applications. PSBMs, particularly those based on finite element methods (FEM), are accurate for simulating organ behaviors, yet their computational intensity has hindered real-time implementation, especially for hyper-elastic tissues. HyperU-Mesh addresses these challenges by integrating Hypernetwork into the U-Mesh architecture. This allows HyperU-Mesh to adapt dynamically to patient-specific biomechanical properties, such as varying stiffness parameters, without the need for retraining. Thus, HyperU-Mesh ensures robust performance in real-world scenarios where precise material parameters are often only available intraoperatively. Our experimental results demonstrated the effectiveness of HyperU-Mesh across different scenarios involving diverse complex material properties and geometries. Highlighting its ability to predict deformations with accuracy comparable to traditional FEM simulations while being real-time at inference. In future work, we will extend the application of HyperU-Mesh to include fixed boundary conditions and geometric variation uncertainties.

References

1. Servin, Frankangel and Collins, Jarrod A. and Heiselman, Jon S. and Frederick-Dyer, Katherine C. and Planz, Virginia B. and Geevarghese, Sunil K. and Brown, Daniel B. and Jarnagin, William R. and Miga, Michael I. Simulation of Image-Guided Microwave Ablation Therapy Using a Digital Twin Computational Model. IEEE Open Journal of Engineering in Medicine and Biology, doi: 10.1109/OJEMB.2023.3345733.
2. Suwelack S, Rohl S, Bodenstedt S, Reichard D, Dillmann R, dos Santos T, Maier-Hein L, Wagner M, Wunscher J, Kenngott H, Muller BP, and Speidel S, “Physics-based shape matching for intraoperative image guidance,” Med Phys. 41(11):111901, 2014.
3. N. Haouchine, J. Dequidt, I. Peterlik, E. Kerrien, M. -O. Berger and S. Cotin, "Image-guided simulation of heterogeneous tissue deformation for augmented reality during hepatic surgery," 2013 IEEE International Symposium on Mixed and Augmented Reality (ISMAR), Adelaide, SA, Australia, 2013, pp. 199-208, doi: 10.1109/ISMAR.2013.6671780.
4. Alvarez P., Chabanas M., Rouz e S., Castro M., Payan Y., and J. L. Dillenseger, “Lung deformation between preoperative ct and intraoperative cbct for thoracoscopic surgery: a case study,” Medical Imaging, Vol. 10576D, 2018.
5. Meier, U., L´opez, O., Monserrat, C. et al. (2005). Real-time deformable models for surgery simulation: a survey. Comput Methods Programs Biomed., 77(3), 183-197
6. Niroomandi, S., Alfaro, I., Cueto, E., Chinesta, F., 2008. Real-time deformable models of non-linear tissues by model reduction techniques. Computer methods and programs in biomedicine, 91(3), 223-231.
7. Niroomandi, S., Gonzalez, D., Alfaro, I., Bordeu, F., Leygue, A., Cueto, E., Chinesta, F., 2013. Real-time simulation of biological soft tissues: a PGD approach. International journal for numerical methods in biomedical engineering, 29(5), 586-600
8. Johnsen, S. F., Taylor, Z. A., Clarkson, M. J., Hipwell, J., Modat, M., Eiben, B., Han, L. , Hu, Y. , Mertzanidou, T. , Hawkes, D. J. Ourselin, S., 2015. NiftySim: A GPU-based nonlinear finite element package for simulation of soft tissue biomechanics. International journal of computer assisted radiology and surgery, 10(7), 1077-1095

9. LeCun Y., Bengio Y., Convolutional Networks for Images, Speech. and Time-series. The handbook of brain theory and neural networks. 3361(10), 1995.
10. Scarselli F., Gori M., A. Tsoi C., Hagenbuchner M. and Monfardini G., "The Graph Neural Network Model," in IEEE Transactions on Neural Networks, vol. 20, no. 1, pp. 61-80, Jan. 2009
11. Roewer-Despres, F., Khan, N., Stavness, I., 2018. Towards finite element simulation using deep learning, 15th International Symposium on Computer Methods in Biomechanics and Biomedical Engineering.
12. Tonutti, M., Gauthier G., and Guang-Zhong Y., 2017. A machine learning approach for real-time modeling of tissue deformation in image-guided neurosurgery. Artificial intelligence in medicine, 80, 39-47.
13. Andrea Mendizabal and Pablo Marquez-Neila and Stephane Cotin. "Simulation of hyperelastic materials in real-time using deep learning", Medical Image Analysis, Volume 59, 2020, ISSN 1361-8415, https://doi.org/10.1016/j.media.2019.101569.
14. El Hadramy, Sidaty and Verde, Juan and Padoy, Nicolas and Cotin, Stéphane. Towards real-time vessel-guided augmented reality for liver surgery. 2024. hal-04387242
15. Ronneberger, O., Fischer, P. and Brox, T. (2015). U-Net: Convolutional Networks for Biomedical Image Segmentation. MICCAI, pp. 234-241
16. Ha, D. and Dai, Andrew M. and V. Le, Quoc. "HyperNetworks", International Conference on Learning Representations (ICLR), 2017.
17. Chauhan, VK and Molaei, S and Clifton, DA and Lu, P and Zhou, J. "A brief review of hypernetworks in deep learning", 2023. https://arxiv.org/abs/2306.06955
18. Ortiz, Jose Javier Gonzalez, John Guttag, and Adrian Dalca. Magnitude Invariant Parametrizations Improve Hypernetwork Learning. arXiv preprint arXiv:2304.07645 (2023).
19. Faure F., Duriez C., Delingette H., Allard J., Gilles B., Marchesseau S., and Cotin S., "Sofa: A multi-model framework for interactive physical simulation," Soft tissue biomechanical modeling for computer-assisted surgery, 283-321, 2012.
20. Mazier, A., El Hadramy, S., Brunet, JN. et al. Sonics: develop intuition on biomechanical systems through interactive error-controlled simulations. Engineering with Computers (2023). https://doi.org/10.1007/s00366-023-01877-w
21. Mazier, A., Bilger, A., Forte, A.E. et al. Inverse deformation analysis: an experimental and numerical assessment using the FEniCS Project. Engineering with Computers 38, 4099–4113 (2022). https://doi.org/10.1007/s00366-021-01597-z
22. Benzley S. E., Perry E., Merkley K., Clark B., and Sjaardama G, "A comparison of all hexagonal and all tetrahedral finite element meshes for elastic and elastoplastic analysis," 4th international meshing roundtable, (17) pp. 179-191., 1995.